

GSC 2314-0530: the shortest-period eclipsing system with dMe components [★]

Dinko P. Dimitrov^{1†} and Diana P. Kjurkchieva²

¹*Institute of Astronomy, Bulgarian Academy of Sciences, 72 Tsarigradsko shossee str., 1784 Sofia, Bulgaria*

²*Department of Physics, Shumen University, 115 Universitetska str., 9700 Shumen, Bulgaria*

Accepted –. Received –; in original form –

ABSTRACT

CCD photometric observations in *VRI* colors and spectroscopic observations of the newly discovered eclipsing binary GSC 2314-0530 (NSVS 6550671) with dMe components and very short period of $P = 0.192636$ days are presented. The simultaneous light-curve solution and radial velocity solution allows to determine the global parameters of GSC 2314-0530: $T_1 = 3735$ K; $T_2 = 3106$ K; $M_1 = 0.51 M_\odot$; $M_2 = 0.26 M_\odot$; $R_1 = 0.55 R_\odot$; $R_2 = 0.29 R_\odot$; $L_1 = 0.053 L_\odot$; $L_2 = 0.007 L_\odot$; $i = 72.5^\circ$; $a = 1.28 R_\odot$; $d = 59$ pc. The chromospheric activity of its components is revealed by strong emission in the $H\alpha$ line (with mean $EW = 5$ Å) and observed several flares. Empirical relations mass– M_{bol} , mass–radius and mass–temperature are derived on the basis of the parameters of known binaries with low-mass dM components.

Key words: binaries: eclipsing – binaries: spectroscopic – stars: activity – stars: fundamental parameters – stars: late-type – stars: low-mass

1 INTRODUCTION

Although the M dwarfs are the most numerous stars in our Galaxy, the mass, metallicity and age dependencies of their stellar luminosities and radii are poorly calibrated. The reason is the selection effect that plays against the detection of fainter and smaller stars.

Less than 20 binaries with low-mass dM components have empirically-determined masses, radii, luminosities and temperatures (see Section 5, Table 6). As a result the mass-luminosity relation is determined by only a few low-mass stars. This deficiency hindered the development of the models for the cool dense atmospheres of the M dwarfs. It is established that all available models underestimate the radii (by around 10–15 per cent) and overestimate the temperatures (by 200–300 K) of short-period binaries with dM components (Ribas 2003; Maceroni & Montalbán 2004).

The Northern Sky Variability Survey (NSVS) contains a great number of photometric data (Wozniak et al. 2004) that allows searching of variable stars and determination of their periods and types of variability. A multiparametric method for search for variable objects in large datasets was tested on the NSVS (Dimitrov 2009) and as a result many eclipsing stars were discovered. One of them was GSC 2314-0530 \equiv NSVS 6550671 ($\alpha=02^{\text{h}}20^{\text{m}}50^{\text{s}}.9$, $\delta=+33^\circ20'46''.6$).

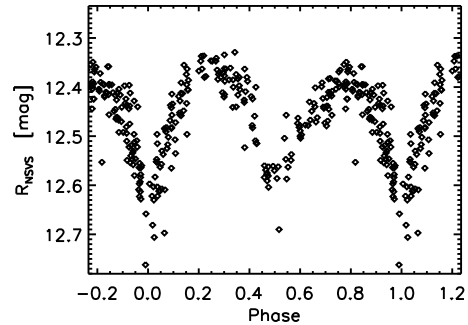


Figure 1. NSVS photometry of GSC 2314-0530

On the base of the NSVS photometry obtained in 1999–2000 we derived the ephemeris:

$$HJD(\text{MinI}) = 2451352.062 + 0.192637 \times E \quad (1)$$

and built its light curve (Fig. 1).

We found that this star has been assigned also as SWASP J022050.85+332047.6 according to the SuperWASP photometric survey (Pollacco et al. 2006). Norton et al. (2007) reported its coincidence with the *ROSAT* X-ray source 1RXS J022050.7+332049.

Initially GSC 2314-0530 attracted our interest by its short orbital period because there were only several systems with non-degenerate components and periods below the short-period limit of 0.22 days (Rucinski 2007):

[★] Based on the data obtained at Rozhen National Astronomical Observatory, and the Northern Sky Variability Survey

[†] E-mail: dinko@astro.bas.bg; d.kjurkchieva@shu-bg.net

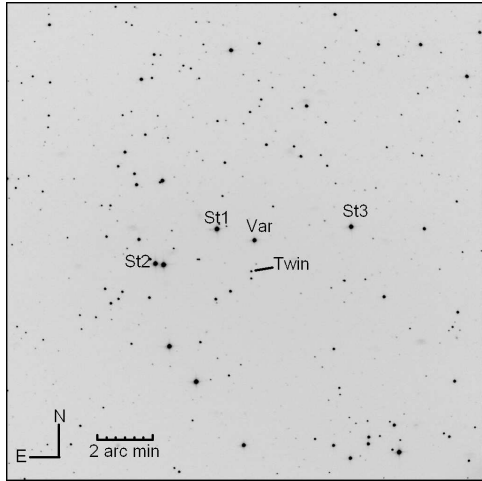


Figure 2. Observed field around GSC 2314-0530

GSC 1387-0475 with $P = 0.217811$ d (Rucinski 2007; Rucinski & Pribulla 2008), ASAS J071829-0336.7 with $P = 0.211249$ d (Pribulla et al. 2009), the star V34 in the globular cluster 47 Tuc with $P = 0.2155$ d (Weldrake et al. 2004) and BW3 V38 with orbital period $P = 0.1984$ d (Maceroni & Rucinski 1997; Maceroni & Montalbán 2004).

When we established that the components of GSC 2314-0530 were dM stars our interest increased and we undertook intensive photometric and spectral observations in order to determine its global parameters and to add a new information for the dM stars as well as for the short-period binaries.

2 OBSERVATIONS AND DATA REDUCTION

2.1 New photometry

The CCD photometry of GSC 2314-0530 in *VRI* bands was carried out at Rozhen National Astronomical Observatory with the 2-m RCC telescope equipped with VersArray CCD camera (1300×1340 pixels, $20 \mu\text{m}$ pixel, field of 5.25×5.35 arcmin) as well as with the 60-cm Cassegrain telescope using the FLI PL09000 CCD camera (3056×3056 pixels, $12 \mu\text{m}$ pixel, field of 17.1×17.1 arcmin). The average photometric precision per data point was $0.005 - 0.008$ mag for the 60-cm telescope and $0.002 - 0.003$ mag for the 2-m telescope. Table 1 presents the journal of our photometric observations.

It should be noted that the observations on 2009 December 30 are synchronous in the *VRI* colors.

Standard stars of Landolt (1992) and standard fields of Stetson (2000) were used for transition from the instrumental system of each telescope to standard photometric system.

The standard IDL procedures (adapted from DAOPHOT) were used for reduction of the photometric data. The standard stars were chosen on the basis of the method of Everett & Howell (2001) and Table 2 presents their colors. The values of $J - K$ are from the catalogue NOMAD (Zacharias et al. 2005) while the values of other parameters are our estimations.

The field of the variable and standard stars is shown in Fig. 2.

Table 3 presents a sample of our photometric data (the

Table 3. BVRI photometry of GSC 2314-0530

HJD	Magnitude	Filter
2455156.329669	14.8530	B
2455156.332679	14.8490	B
2455156.335689	14.8300	B
2455126.417320	13.3610	V
2455126.418512	13.3618	V
2455126.419890	13.3619	V
2455126.420167	13.3624	V
2455126.420700	13.3547	V
2455126.420978	13.3583	V
2455126.421128	13.3609	V

full table is available in the online version of the article, see Supporting Information).

Some of our photometric runs covering well the orbital cycle are presented in Fig. 3.

The Fourier analysis of all our photometric data performed by the software PERIOD-04 (Lenz & Breger 2005) leads to the ephemeris:

$$HJD(\text{MinI}) = 2451352.061633 + 0.1926359 \times E. \quad (2)$$

The new-obtained period value is almost the same as that of the ephemeris (1) of the NSVS data that means that the orbital period of GSC 2314-0530 is stable.

The color indices of our target (Table 2) lead to M spectral type of the binary. Taking into account the almost equal eclipse depths of the light curve, i.e. the close temperatures of the components, as well as the short orbital period of the system, we may conclude that the two components of GSC 2314-0530 are dM stars.

The value of the obtained period is below the short-period limit and reveals that our target is the shortest-period binary with dM components.

Figure 4 shows the folded light curves from all our photometric data phased according to the ephemeris (2).

2.2 Spectroscopy

We obtained 26 spectra of GSC 2314-0530 with resolution 0.19 \AA/pixel during November – December 2009 covering spectral range of 200 \AA around the $\text{H}\alpha$ line. We used a CCD Photometrics AT200 camera with the SITe SI003AB 1024×1024 pixels chip mounted on the Coude spectrograph (grating B&L632/14.7°) on the 2-m RCC telescope at Rozhen.

The exposure time was 15 min during 2009 November 26 and 20 min during 2009 December 31 and 2010 January 01. All stellar integrations were alternated with Th-Ar comparison source exposures for wavelength calibration. The bias frames and flat-field integrations were obtained at the beginning and at the end of the night. The mean S/N ratio for our observations was around 24, i.e. acceptable for radial velocity determination. Table 4 presents the journal of our spectral observations.

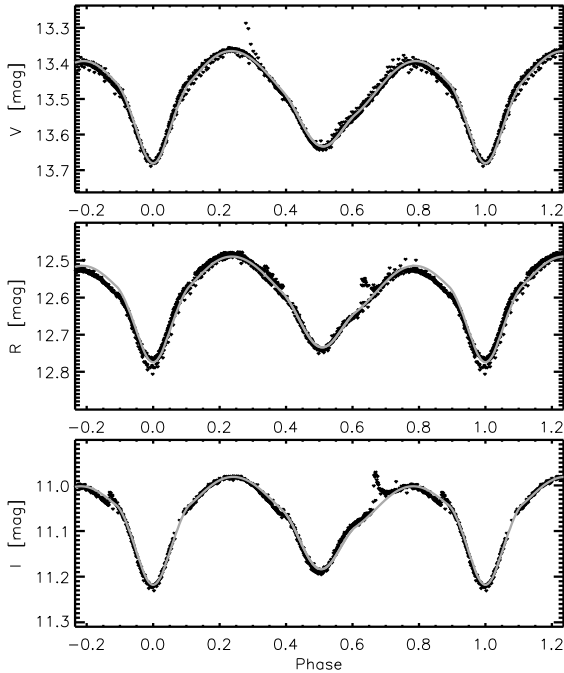
The reduction of the spectra was performed using IRAF packages by bias subtraction, flat fielding, cosmic ray removal, one-dimensional spectrum extraction and wavelength calibration. Figure 5 illustrates the orbital variability of the star spectra while Figure 6 presents the one-dimensional $\text{H}\alpha$ profiles at some orbital phases.

Table 1. Journal of the photometric observations

Date	HJD(start)	Phases	Filter	Exp. [s]	N	Telescope
2009 July 25	2455038.482662	0.725 – 1.298	<i>R</i>	120	126	60-cm
2009 July 26	2455039.484907	0.927 – 0.491	<i>R</i>	120	54	60-cm
2009 July 27	2455040.468322	0.032 – 0.693	<i>R</i>	120	83	60-cm
2009 July 28	2455041.501250	0.395 – 0.881	<i>R</i>	120	62	60-cm
2009 Oct. 21	2455126.412740	0.210 – 1.294	<i>V</i>	15	737	2-m
2009 Nov. 13	2455149.178102	0.393 – 1.389	<i>I</i>	10	850	2-m
2009 Nov. 13	2455149.375822	0.419 – 1.391	<i>R</i>	10	835	2-m
2009 Nov. 20	2455156.324421	0.489 – 0.521	<i>B</i>	120	3	60-cm
2009 Nov. 20	2455156.325521	0.495 – 1.862	<i>V</i>	60	183	60-cm
2009 Nov. 20	2455156.326088	0.498 – 0.529	<i>R</i>	30	3	60-cm
2009 Nov. 20	2455156.326493	0.500 – 0.531	<i>I</i>	30	3	60-cm
2009 Dec. 30	2455196.225416	0.610 – 1.785	<i>V</i>	120	65	60-cm
2009 Dec. 30	2455196.226516	0.616 – 1.791	<i>R</i>	60	65	60-cm
2009 Dec. 30	2455196.227256	0.619 – 1.810	<i>I</i>	60	65	60-cm

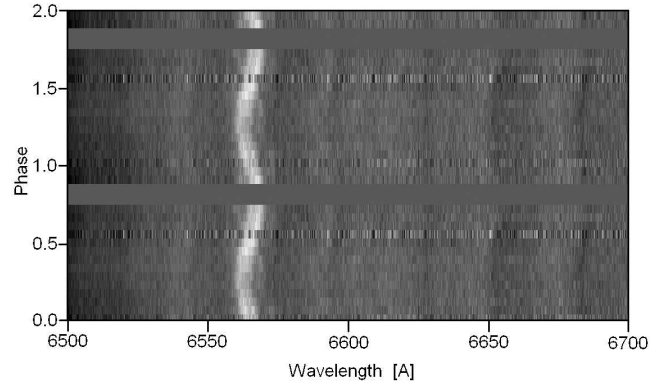
Table 2. Colors and proper motion of the variable star and standard stars

	ID	<i>V</i>	<i>B</i> – <i>V</i>	<i>V</i> – <i>R</i>	<i>V</i> – <i>I</i>	<i>J</i> – <i>K</i>	pmRA	pmDE
	GSC/USNO-B1	[mag]	[mag]	[mag]	[mag]	[mag]	[mas yr ⁻¹]	[mas yr ⁻¹]
Var	2314-0530	13.36	1.18	0.88	2.38	0.87	144.0	-112.0
St1	2314-1784	12.12	0.30	0.25	0.57	0.29	-000.8	-008.3
St2	2314-1378	12.24	0.29	0.24	0.58	0.34	-000.1	-001.6
St3	2314-1655	12.40	0.22	0.20	0.46	0.27	005.5	-004.0
Twin	1233-0046425	16.91	1.41	1.03	3.02	0.87	140.0	-112.0

**Figure 4.** The folded *V*, *R*, *I* light curves of GSC 2314-0530 and their fits

3 ANALYSIS OF THE SPECTRAL DATA

The obtained spectra of GSC 2314-0530 show wide emission $H\alpha$ lines implying high rotational velocities as well as absorption TiO bands at 6569 Å and 6651 Å (Fig. 5). These

**Figure 5.** The orbital variability of the spectra of GSC 2314-0530 from 2009 November 26

spectral features suggest a dMe classification of GSC 2314-0530.

The spectral contribution of the secondary component is visible only in the $H\alpha$ line (Fig. 5). That is why we determined the radial velocities of the two stellar components by fitting the $H\alpha$ lines at each phase with Gaussians (Fig. 7).

Table 4 and Figure 8 present the radial velocities of the stellar components of GSC 2314-0530. Their fit corresponds to values $K_1 = V_1 \sin i = 109.7 \pm 3.2 \text{ km s}^{-1}$, $K_2 = V_2 \sin i = 211.3 \pm 5.8 \text{ km s}^{-1}$ and $V_0 \sin i = -1.2 \pm 5.7 \text{ km s}^{-1}$. They lead to mass ratio $q = 0.519 \pm 0.029$ and binary separation $a \sin i = 1.22 \pm 0.04 R_\odot$.

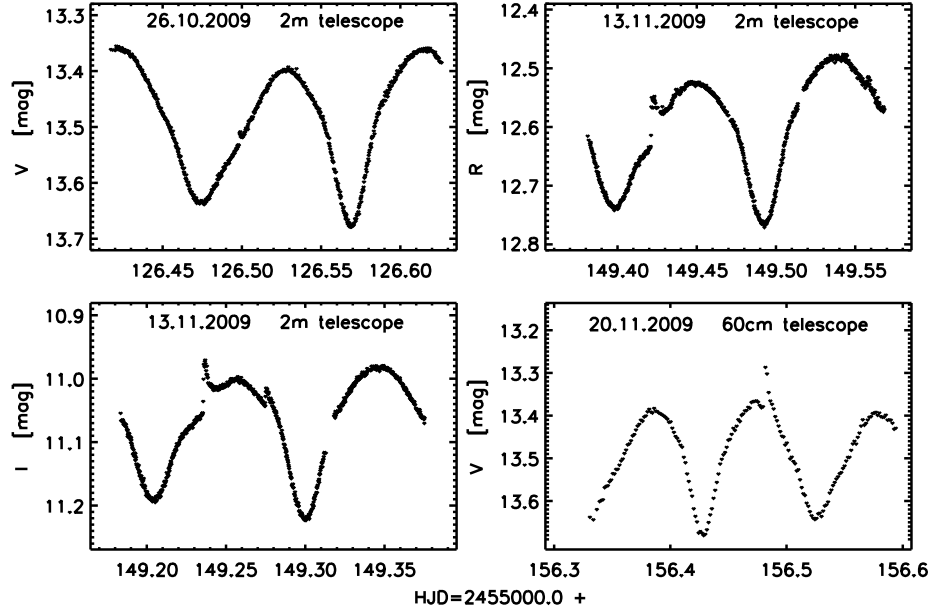


Figure 3. The photometric observations of GSC 2314-0530 from 2009 October 26, 2009 November 13 and 2009 November 20

Table 4. Journal of the spectral observations and parameters of the $H\alpha$ lines

No	HJD	S/N	phase	RV_1 [km s ⁻¹]		RV_2 [km s ⁻¹]		EW_{total} [Å]
01	2455162.375293	23	0.88	89.2	±3.3	-157.5	±6.2	4.97
02	2455162.385975	19	0.93	42.8	±3.7			4.56
03	2455162.396657	22	0.99	-9.3	±6.6			3.61
04	2455162.407335	21	0.04	-57.9	±4.5	63.0	±4.0	6.64
05	2455162.418012	27	0.10	-68.0	±4.5	99.1	±10.8	4.34
06	2455162.428689	28	0.15	-92.8	±3.2	210.3	±9.3	4.04
07	2455162.439367	28	0.21	-116.6	±4.4	165.8	±6.9	3.53
08	2455162.450048	29	0.27	-120.7	±4.6	174.0	±7.9	3.62
09	2455162.460726	28	0.32	-86.7	±2.6	187.1	±3.2	4.60
10	2455162.471405	30	0.38	-81.6	±4.3	176.4	±4.9	4.49
11	2455162.482903	25	0.44	-48.4	±2.2			5.47
12	2455162.493582	26	0.49	-0.6	±3.8			5.55
13	2455162.514939	25	0.60	73.4	±5.6	-106.5	±12.9	5.34
14	2455162.526143	24	0.66	93.8	±4.1	-170.6	±5.9	4.94
15	2455162.537036	25	0.72	96.2	±3.4	-222.2	±8.6	6.18
16	2455197.222839	18	0.78	120.7	±7.4			5.92
17	2455197.236667	29	0.85	93.9	±3.0	-160.6	±9.1	5.07
18	2455197.250817	27	0.92	48.6	±4.4	-123.3	±4.5	5.34
19	2455197.264965	28	0.99	-37.1	±4.9			5.59
20	2455197.279111	27	0.07	-60.1	±3.0			5.67
21	2455197.293257	29	0.14	-91.7	±4.8	198.2	±10.0	4.16
22	2455197.308131	29	0.22	-119.1	±4.3	212.2	±7.8	4.44
23	2455197.322278	30	0.29	-101.8	±2.9	191.2	±6.1	3.76
24	2455197.336431	28	0.37	-75.4	±4.0	168.5	±6.1	3.65
25	2455198.274197	25	0.23	-91.5	±3.4	205.3	±4.3	6.04
26	2455198.288351	25	0.31	-72.2	±4.0	199.8	±4.0	6.29

4 ANALYSIS OF THE PHOTOMETRIC DATA

The qualitative analysis of the new photometric data (Fig. 4) leads to several conclusions.

(1) The Min I is deeper than Min II. This means that the

secondary's temperature is lower than the primary's temperature.

(2) The light maxima are not equal. This O'Connell effect implies presence of surface temperature spot(s).

(3) The Max I appears at the expected phase 0.25 while the phase of Max II is around 0.78. As a result the second half of

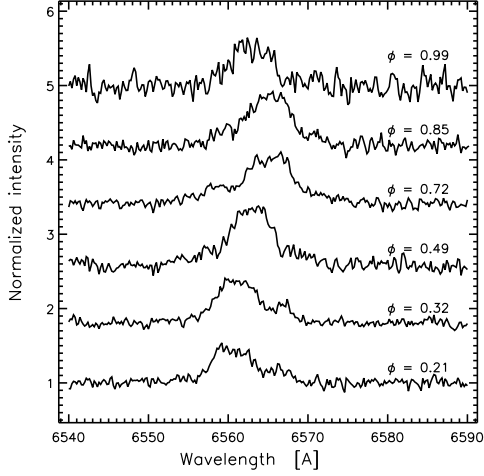


Figure 6. The $H\alpha$ profiles at some phases

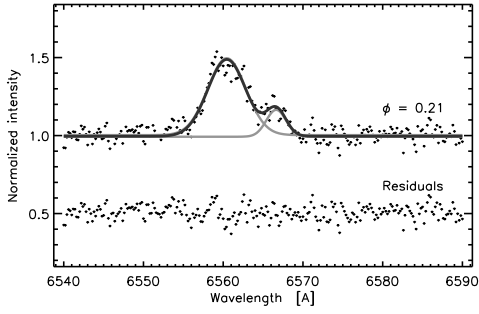


Figure 7. The two Gaussians (gray lines) reproducing the $H\alpha$ line (dots) of the two stellar components, and their sum (black line) fitting the total $H\alpha$ profile of GSC 2314-0530.

the light curves is quite distorted. Similar asymmetry is visible also on the NSVS light curve (Fig. 1) of the star almost 10 years earlier, i.e. this distortion is possibly permanent. We noted that the shape of the light curve of GSC 2314-0530 at phase range 0.5–0.8 resembles at some degree that of the cataclysmic stars with their peculiar standstills causing delay of the light increasing after the light minimum.

(4) The $V-I$ light curve of GSC 2314-0530 (Fig. 9) clearly reveals that the system becomes redder after the two eclipses and bluer after the two quadratures. The phases of the ex-

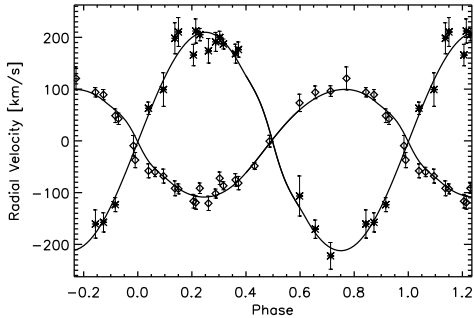


Figure 8. Radial velocities of the two components of GSC 2314-0530 (the sizes of the error bars correspond to 3σ) and their fits by the code PHOEBE (Prša & Zwitter 2005).

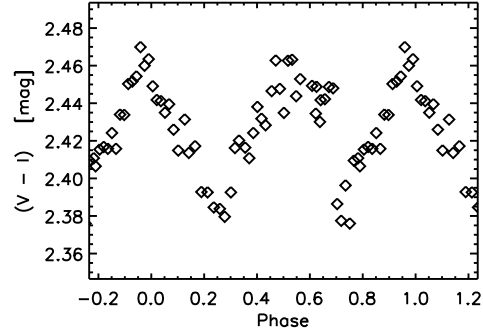


Figure 9. $V-I$ light curve of GSC 2314-0530 from synchronous VRI observation with 60-cm telescope

trema of the $V-I$ light curve have around 0.05 phase delays in respect to those of the light curves **except** for the second maximum of $V-I$ which delay is more than 0.10.

(5) We observed several flares of GSC 2314-0530 (Fig. 3) resembling those of UV Ceti stars (see more in Section 6).

In order to determine the global parameters of GSC 2314-0530 we modeled our VRI folded curves simultaneously using the software PHOEBE (Prša & Zwitter 2005) by the following procedure.

(a) We fixed the mass ratio $q = 0.519$ from our radial velocity solution.

(b) The obtained components of the heliocentric space velocity $U = -23$ km/s, $V = -44$ km/s and $W = -12$ km/s allow us to assume solar metallicity for the emission of GSC 2314-0530 (Leggett 2000).

(c) We adopted coefficients of gravity brightening $g_1 = g_2 = 0.32$ and reflection $A_1 = A_2 = 0.5$ (appropriate for late stars) while the limb-darkening coefficients for each star and each color were taken from the tables of van Hamme (1993).

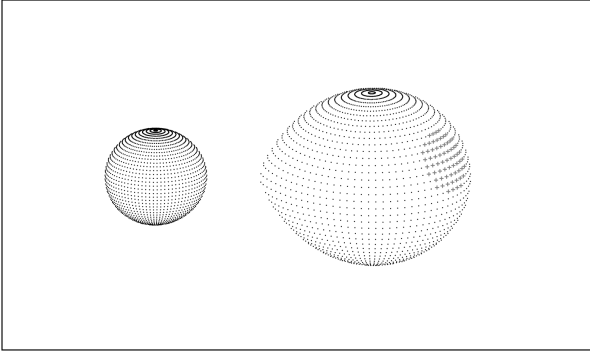
(d) Taking into account that $E(V-I) = 0.03$ mag in the GSC 2314-0530' direction (Schlegel et al. 1998) we obtained its de-reddened color index $(V-I)_0 = 2.35$ mag. According to table 2 of VandenBerg & Clem (2003) this out-of-eclipse color index corresponds to mean temperature of the binary $T_m = 3560$ K.

It should be noted that the index $B-V = 1.18$ mag of GSC 2314-0530 corresponds to mean temperature around 4400 K, i.e. 840 K higher than that obtained by the $V-I$ index. This is a new confirmation of the conclusion that the majority of the dMe stars have $B-V$ colors too blue for their $V-I$ colors (Stauffer & Hartmann 1986). Our result also shows that the temperature difference obtained by the two color indices ($V-I$ and $B-V$) is higher than 200–300 K (Ribas 2003; Maceroni & Montalbán 2004) and can reach 800 K.

(e) At the first stage we fixed $T_1 = 3700$ K (taking into account that the temperature of the primary component T_1 is higher than T_m) and varied the secondary' temperature T_2 , the orbital inclination i and the potentials $\Omega_{1,2}$. In order to reproduce the O'Connell effect and light curve distortions we had to add two cool spots on the primary's surface and to vary their parameters: longitude λ , latitude β , angular size α and temperature T_{sp} .

Table 5. Best light curve solution from PHOEBE

Parameter		Value	
i	[°]	72.5	± 0.1
T_1	[K]	3735	± 10
T_2	[K]	3106	± 10
Ω_1		2.944	± 0.002
Ω_2		3.545	± 0.009
λ_{Sp1}	[°]	147	± 5
β_{Sp1}	[°]	70	± 10
α_{Sp1}	[°]	20	± 1
T_{Sp1}	[K]	3175	± 50
λ_{Sp2}	[°]	195	± 5
β_{Sp2}	[°]	75	± 10
α_{Sp2}	[°]	8	± 1
T_{Sp2}	[K]	3175	± 50
$L_3(V)$		0.171	± 0.003
$L_3(R)$		0.222	± 0.002
$L_3(I)$		0.298	± 0.002

**Figure 10.** 3D model of GSC 2314-0530 at phase 0.75

Moreover, in order to get a good simultaneous fit for the three colors *VRI* by the same stellar and spot parameters we added a third light L_3 which contributes differently to the different colors. We consider the last supposition as artificial step to compensate the peculiar energy distribution of the dM stars that appear especially faint in the *V* band probably to the big TiO absorption as well as to the big contribution of the spots.

(f) After getting a good fit of our *VRI* photometric data we began to vary also the primary's temperature. As a result we obtained the best light curve solution which parameters are given in Table 5. The respective synthetic *VRI* light curves are shown in Fig. 4 as gray lines. They coincide very well with the observational data at all phases except for the flares.

The obtained potentials correspond to relative mean stellar radii $r_1 = 0.431$ and $r_2 = 0.228$ revealing that the primary component almost fills-in its Roche lobe (Fig. 10).

5 GLOBAL PARAMETERS OF GSC 2314-0530

Using the photometric value of the orbital inclination $i = 72.5^\circ$ we determined consecutively the following global parameters of GSC 2314-0530:

- (a) orbital velocities of the two components $V_1 = 115.1 \pm 3.4 \text{ km s}^{-1}$, $V_2 = 221.6 \pm 6.1 \text{ km s}^{-1}$;
- (b) orbital separation $a = 1.28 \pm 0.04 R_\odot$;
- (c) masses of the components $M_1 = 0.51 \pm 0.02 M_\odot$ and $M_2 = 0.26 \pm 0.02 M_\odot$;
- (d) absolute (mean) radii of the components $R_1 = 0.55 \pm 0.01 R_\odot$ and $R_2 = 0.29 \pm 0.01 R_\odot$;
- (e) surface gravity $\log g_1 = 4.68$ and $\log g_2 = 4.95$;
- (f) stellar luminosities $L_1 = 0.053 \pm 0.002 L_\odot$ and $L_2 = 0.0070 \pm 0.0006 L_\odot$;
- (g) bolometric absolute magnitudes of the components (using $M_{\text{bol}}^\odot = 4.72$) $M_{\text{bol1}} = 7.91 \pm 0.04 \text{ mag}$ and $M_{\text{bol2}} = 10.11 \pm 0.09 \text{ mag}$ as well as bolometric absolute magnitude of the binary $M_{\text{bol}}(\text{total}) = 7.77 \pm 0.05 \text{ mag}$;
- (h) absolute *V* magnitude of the binary $M_V(\text{total}) = 9.5 \pm 0.05 \text{ mag}$ (using $BC_V = -1.73$ corresponding to T_m from table 2 of Vandenberg & Clem 2003);
- (i) distance to the binary $d = 59 \pm 2 \text{ pc}$.

It should be noted that while the masses and radii of the components were directly determined, their temperatures and absolute magnitudes required external calibrations which are poorly known for the late stars.

We calculated the equatorial velocities of the components by measuring the rotation broadening of their H α lines (using $i = 72.5^\circ$). The obtained values $V_{\text{rot1}} = 145 \pm 15 \text{ km s}^{-1}$ and $V_{\text{rot2}} = 69 \pm 15 \text{ km s}^{-1}$ reveal that the components of GSC 2314-0530 are quite fast rotators (see Table 7). Thus our target confirms the conclusion of Stauffer & Hartmann (1986) that the stars with larger velocities have centrally peaked H α emission while the slower rotators have centrally reversed profiles as well as the conclusion of Worden et al. (1981) that stars with centrally peaked H α emission profiles belong to short-period binaries.

Some of the determined global parameters of GSC 2314-0530 together with those of the other known binaries with low-mass dM components are given in Table 6 which columns are: star name; period P in days; temperatures T of the components; masses M , radii R and luminosities L of the components in solar units; orbital inclination i in degrees; mass ratio q ; color index $V-I$ of the binary; bolometric absolute magnitudes M_{bol} of the components; orbital separation a in solar radii; distance d in pc; type of binary configuration (D – detached, SD – semidetached); references.

Figure 11 shows the empirical diagrams mass- M_{bol} , mass-radius and mass-temperature for the low-mass stars from Table 6 (total number 34). They occupy relative narrow bands on these diagrams. This means that the luminosities, radii and temperatures of these stars depend on their masses. These statistical relations can be described by the following formulas:

$$\begin{aligned}
 M_{\text{bol}} &= 13.0 - 13.4 \times M + 7.7 \times M^2 \\
 R &= 0.019 + 1.002 \times M \\
 T &= 2983 + 396 \times M + 1333 \times M^2
 \end{aligned} \tag{3}$$

We assume that the bigger scatter of the mass-temperature diagram is due mainly to the weakly established calibration $T/(V-I)$ for the late low-mass stars. Moreover, some star temperatures probably have been determined without taking into account the reddening.

Table 6. Parameters of binaries with low-mass dM components

Name	P [d]	T [K]	M [M_{\odot}]	R [R_{\odot}]	L [L_{\odot}]	i [$^{\circ}$]	q	$V-I$ [mag]	M_{bol} [mag]	a [R_{\odot}]	d [pc]	Type	Ref.
CU Cnc=GJ 2069A	2.77	3160	0.43	0.43	0.016	86	0.92	2.80	9.19	0.92	12.8	D	(1)
		3125	0.40	0.39	0.013				9.45				
2MASS J01542930+0053266	2.64	3700	0.66	0.64	0.069	86	0.95		7.62	8.70	623	D	(2)
		3300	0.62	0.61	0.039				8.24				
NSVS 06507557	0.51	3960	0.65	0.60	0.079	83	0.42	2.13	7.48	2.65	111	D	(3)
		3360	0.28	0.44	0.022				8.86				
NSVS 07394765	2.26	3170	0.56	0.58	0.030	84	1.16		8.52	2.60		D	(4)
		3860	0.65	0.69	0.095				7.27				
NSVS 07453183	0.37	3340	0.68	0.72	0.060	89	1.07	1.40	7.77	7.75		D	(4)
		3570	0.73	0.79	0.090				7.33				
UNSW-TR-2	2.11	3870	0.53	0.64	0.082	83	0.95		7.43	7.05	169	D	(5)
		3845	0.51	0.61	0.073				7.56				
CM Dra	1.27	3150	0.23	0.25	0.005	90	0.93		10.47	3.75		D	(6)
		3125	0.21	0.23	0.004				10.71				
TrES HerO-07621	1.12	3500	0.49	0.45	0.027	83	0.95		8.64	2.25	118	D	(7)
		3400	0.49	0.45	0.024				8.77				
YY Gem	0.81	3820	0.60	0.62	0.070	86	1.00	1.92	7.57	3.87		D	(8)
		3820	0.60	0.62	0.070				7.57				
GJ 3226	0.77	3313	0.38	0.37	0.016	83	0.75	2.73	9.20	3.08	42	D	(9)
		3247	0.28	0.32	0.009				9.83				
2MASS 04463285+1901432	0.62	3320	0.47	0.56	0.034	81	0.41	2.59	8.39	2.66	540	D	(10)
		2910	0.19	0.21	0.003				11.03				
V405 And	0.496	4050	0.49	0.78	0.147	66	0.98		6.80	2.25		D	(11)
		3000	0.21	0.23	0.004				10.71				
GU Boo	0.49	3920	0.61	0.62	0.082	88	0.98	1.90	7.43	2.79	100	D	(12)
		3810	0.60	0.62	0.073				7.60				
SDSS MEB-1	0.41	3320	0.27	0.27	0.008	85	0.98		9.96	1.85		D	(13)
		3300	0.24	0.25	0.007				10.11				
NSVS 01031772	0.37	3615	0.54	0.53	0.043	86	0.92		8.08	2.20	40	D	(14)
		3513	0.50	0.51	0.036				8.27				
OGLE BW3 V38	0.198	3500	0.44	0.51	0.035	86	0.95	2.45	8.39	1.35	400	SD	(15)
		3450	0.41	0.44	0.025				8.78				
GSC 2314-0530	0.192	3735	0.51	0.55	0.053	72	0.52	2.34	7.91	1.28	59	SD	(16)
		3106	0.26	0.29	0.007				10.11				

References: (1) Ribas 2003, Delfosse et al. 1999; (2) Becker et al. 2008; (3) Cakirli & Ibanoglu 2009; (4) Coughlin & Shaw 2007; (5) Young et al. 2006; (6) Metcalfe et al. 1996; (7) Creevey et al. 2005; (8) Bopp 1974, Torres & Ribas 2002; (9) Irwin et al. 2009; (10) Hebb et al. 2006; (11) Vida et al. 2008; (12) Lopez-Morales & Ribas 2005; (13) Blake et al. 2008; (14) Lopez-Morales et al. (2006); (15) Maceroni & Montalbán (2004); (16) this paper

6 ACTIVITY OF GSC 2314-0530

The manifestations of stellar activity as H α emission, spots, flares, etc., are consequences of magnetic fields. It is assumed that the fully-convective late stars have strong, long-lasting, magnetic field.

According to Mullan & MacDonald (2001) the larger radii and lower temperatures of dM stars can be explained by the presence of strong magnetic fields and their activity is at the saturation limit. Perhaps the significant spot coverage decreases the photospheric temperature which the star compensates by increasing its radius to conserve the total radiative flux.

6.1 Surface spots

The photospheric activity of the late stars is demonstrated mainly by O'Connell effect and distorted light curves. They can be reproduced by surface temperature inhomogeneities (spots). It is reasonable to assume existence of cool spots by analogy with our Sun. Usually they are put on the primary

star although the same effect can be reached by spots on the secondary but then the spots should be larger and/or cooler. There are also fits of the light curves of late binaries with bright spots (Torres & Ribas 2002; Maceroni et al. 1994). These are interpreted by uniform distribution of dark spots covering however most of stellar surface except for a spot-free area, i.e. "bright spots" represent the true photosphere.

The light curves of all binaries with low-mass dM components from Table 6 are distorted and they have been reproduced by large cool spots which angular radii reach up to 80 $^{\circ}$.

The distorted light curves of GSC 2314-0530 were reproduced by two cool spots on the primary component (see their parameters in Table 5) covering 3.5 per cent of its surface. The fact that the shape of the light curve distortions of GSC 2314-0530 remains the same almost 10 years means that the main (larger) spot visible at phase 0.6 presents long-lived active region on the primary surface.

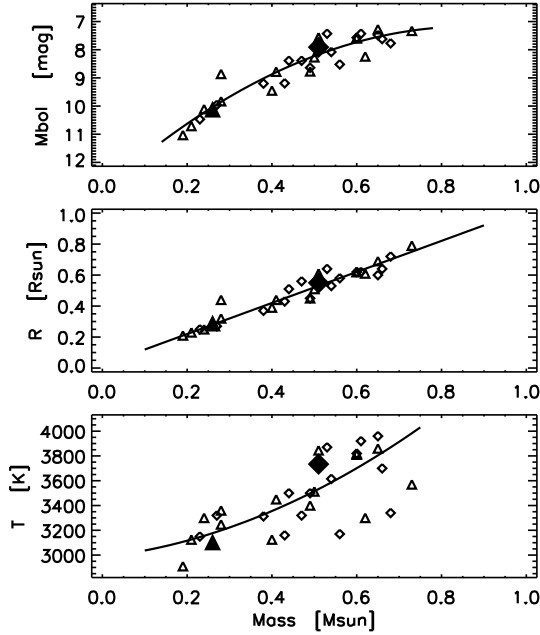


Figure 11. Empirical relations mass- M_{bol} , mass-radius and mass-temperature for the low-mass stars from Table 6 and their fits. The locus of the primary stars are signed by diamonds, those of the secondaries – by triangles, while those of our star – by large filled symbols.

6.2 H α emission

The EW of the H α line is an useful indicator of chromospheric activity for M dwarfs because those stars are much brighter at 6500 Å than at 3900 Å. Stauffer & Hartmann (1986) divided dM into 4 subsets ordered by chromospheric activity. The least chromospheric active dM have weak H α absorption line. As the chromosphere increases the EW of the H α absorption first increases, then decreases and finally H α goes into the emission.

Table 4 presents the orbital variations of the EW of the total H α emission of GSC 2314-0530. Although it seemed to change irregularly in the range 3.6-6.6 Å during the cycle we noted a trend of the EW to be smaller around the first quadrature than around the second quadrature. The exceptions from this trend are the big EW values of the only two spectra from 2010 January 01 at phases 0.23 and 0.31. They may due to flare event. Such a supposition is reasonable because two of the observed flares are around the first quadrature (see Table 8).

The foregoing trend of the H α emission is opposite to that of total light of GSC 2314-0530 that is bigger at the first quadrature than at the second one. Such an anti-correlation is typical for the chromospherically active stars of types RS CVn and BY Dra.

Table 7 presents the EW of the H α emission of some binaries with low-mass dM components from Table 6 at normal state (out of flare). The comparison reveals the strong H α emission of GSC 2314-0530. This result is not surprising taking into account the low temperature and fast rotation of its components.

The mean value $EW = 5$ Å of the H α emission of GSC 2314-0530 is considerably smaller than that of the ac-

Table 7. Activity of low-mass dM stars

Star	V_{rot1} [km s $^{-1}$]	V_{rot2} [km s $^{-1}$]	EW [Å]	Flares
CM Dra			em	Y
CU Cnc			4	
V405 And				Y
GU Boo	64	64	1.7	
YY Gem	37	37	2	Y
NSVS 06507557	59	43	[-3,+2]	
NSVS 01031772	72	70		
BW3 V38	131	113	5.4	
GJ3236	25	19		
GSC 2314-0530	145	69	≤ 6.6	Y

Table 8. Observed flares of GSC 2314-0530

Date	HJD $_{\text{max}}$ 2455000+	Phase	Filter	A [mag]	τ [min]
2009 Oct. 26	126.49373	0.61	V	0.022	4
2009 Nov. 13	149.23146	0.64	I	0.085	22
2009 Nov. 13	149.26995	0.84	I	0.027	13
2009 Nov. 13	149.41788	0.61	R	0.085	19
2009 Nov. 13	149.55281	0.31	R	0.015	9
2009 Nov. 20	156.48180	0.31	V	0.092	25

creting pre-main-sequence dMe stars which H α emission has $EW > 10$ Å.

6.3 Flares

Flare activity is typical for the late stars. The last column of Table 7 shows those stars from our Table 6 in which some flares have been registered (signed by “Y”).

During our observational runs we were witnesses of six flares of GSC 2314-0530 that revealed its high flare activity. The amplitudes A and durations τ of the observed flares are given in Table 8.

It should be noted that 3 of the observed 6 flares occurred around the phase of maximum visibility 0.6 of the large, stable spot (Sp1). This implies correlation between the two signs of stellar activity: spots and flares. Both of them are appearances of the long-lived active area on the primary star.

Besides the optical flares there is information about X-flares of GSC 2314-0530 (Fuhrmeister & Schmitt 2003).

6.4 Angular momentum

The small orbital angular momentum is characteristic feature of all short-period systems ranging from CVs to CB that seem to be old, being at later stages of the angular momentum loss evolution as a result of the period decrease.

We calculated the orbital angular momentum of the target by the expression (Popper & Ulrich 1977)

$$J_{\text{rel}} = M_1 M_2 \left(\frac{P}{M_1 + M_2} \right)^{1/3} \quad (4)$$

where P is in days and M_i are in solar units.

The obtained value $\log J_{\text{rel}} = -1.01$ of GSC 2314-0530

is considerably smaller than those of the RS CVn binaries and detached systems which have $\log J_{\text{rel}} \geq +0.08$. The orbital angular momentum of GSC 2314-0530 is smaller even than those of the contact systems which have $\log J_{\text{rel}} \geq -0.5$. It is bigger only than those of the short-period CVs of SU UMa type.

The small orbital angular momentum of GSC 2314-0530 implies existence of past episode of angular momentum loss during the binary evolution. It means also that GSC 2314-0530 is not pre-MS object. This conclusion is supported by the values of $\log g$ of its components.

6.5 X-ray emission

The X-ray emission of the stellar coronae are directly related to the presence of magnetic fields and consequently gives information about the efficiency of the stellar dynamo.

Rucinski (1984) established that the X-ray luminosity decreased for later M stars while the ratio L_X/L_{bol} did not change significantly from M0 to M6. As a result he proposed the ratio L_X/L_{bol} as most relevant measure of activity of M dwarfs. Vilhu & Walter (1987) found that the upper boundary of L_X/L_{bol} for late M stars is $\sim 10^{-3}$.

Besides all indicators of stellar activity in the optical (surface inhomogeneities, emission lines, flares) the star GSC 2314-0530 shows also X-ray emission (it is identified as ROSAT X-ray source 1RXS J022050.7+332049) and X-ray flares.

On the basis of the measured X-ray flux $F_X = 4.266 \times 10^{-13} \text{ ergs cm}^{-2} \text{ s}^{-1}$ of GSC 2314-0530 at quiescence (Voges et al. 1999; Schmitt et al. 1995) and derived distance 59 pc we calculated its X-ray luminosity $L_X = 1.68 \times 10^{29} \text{ ergs s}^{-1}$. This value is at the upper boundary $\log L_X \approx 29$ for dM stars (Rosner et al. 1981; Caillault et al. 1986). The value $f_X/f_{\text{bol}} = L_X/L_{\text{bol}} = 0.7 \times 10^{-3}$ of GSC 2314-0530 is almost at the upper boundary of this ratio and considerably bigger than those of the M dwarfs studied by Rucinski (1984) and Caillault et al. (1986).

It is known that the activity and angular momentum loss tend to be saturated at high-rotation rates (Vilhu & Walter 1987). Due to its short period and high activity GSC 2314-0530 is perhaps an example of such saturation.

7 IS GSC 2314-0530 ALONE?

Our observed field (Fig. 2) contains the weak star USNO-B1 1233-0046425. We called it Twin due to the same tangential shift as our target star GSC 2314-0530. Table 2 presents the proper motion and the colors of Twin according to the catalogue NOMAD. USNO-B1 1233-0046425 has $V - I = 3.02$ corresponding to temperature less than 3200 K.

We suspect that our "twins" may form visual binary. The angular distance between them of 61 arcsec corresponds to linear separation around 3500 au for distance of 59 pc. Such a supposition is reasonable because it is known that the short-period close binaries often are triple systems (Pribulla & Rucinski 2006). Particularly, the object TrES Her0-07621 from our Table 6 has a red stellar neighbor at a distance 8 arcsec with close proper motion (Creevey 2005).

The check of the supposition if Twin is physical companion of GSC 2314-0530 needs astrometric observations of the "twins".

8 CONCLUSIONS

The analysis of our photometric and spectral observations of the newly discovered eclipsing binary GSC 2314-0530 allows us to derive the following conclusions:

(1) This star is the shortest-period binary with dM components which period is below the short-period limit.

(2) By simultaneous radial velocity solution and light curve solution we determined the global parameters of GSC 2314-0530: inclination $i = 72.5^\circ$; orbital separation $a = 1.28 R_\odot$; masses $M_1 = 0.51 M_\odot$ and $M_2 = 0.26 M_\odot$; radii $R_1 = 0.55 R_\odot$ and $R_2 = 0.29 R_\odot$; temperatures $T_1 = 3735 \text{ K}$ and $T_2 = 3106 \text{ K}$; luminosities $L_1 = 0.053 L_\odot$ and $L_2 = 0.007 L_\odot$; distance $d = 59 \text{ pc}$.

(3) We derived empirical relations mass- M_{bol} , mass-radius and mass-temperature on the basis of the parameters of known binaries with low-mass dM components.

(4) The distorted light curve of GSC 2314-0530 were reproduced by two cool spots on the primary component. The next sign of the activity of GSC 2314-0530 is the strong H α emission of its components. Moreover we registered 6 flares of GSC 2314-0530. Half of them occurred at the phases of maximum visibility of the larger stable cool spot on the primary.

The analysis of all appearances of magnetic activity revealed existence of long-lived active area on the primary of GSC 2314-0530. The high activity of the target is natural consequence of the fast rotation and low temperatures of its components.

Our study of the newly discovered short-period eclipsing binary GSC 2314-0530 presents a next small step toward understanding dMe stars and adds a new information to the poor statistic of the low-mass dM stars. Recently they became especially interesting as appropriate targets for planet searches due to the relative larger transit depths.

ACKNOWLEDGMENTS

The research was supported partly by funds of projects DO 02-362 of the Bulgarian Scientific Foundation. This research make use of the SIMBAD and VizieR databases, operated at CDS, Strasbourg, France, and NASA's Astrophysics Data System Abstract Service. The authors are very grateful to the anonymous referee for the valuable notes and advices.

REFERENCES

- Becker A. et al., 2008, MNRAS, 386, 416
- Blake C. et al., 2008, AJ, 684, 635
- Bopp B.W., 1974, ApJ, 193, 389
- Caillault J. et al., 1986, ApJ, 304, 318
- Cakirly O., Ibanoglu C., 2010, MNRAS, 401, 1141
- Coughlin J., Shaw J., 2007, J. of Southeastern Assoc. for Res. in Astr., 1, 7
- Creevey O., Benedict G., Brown T. et al., 2005, ApJL, 625, 127

- Delfosse X. et al., 1999, A&A, 341, L63
Dimitrov D.P., 2009, BulgAJ, 12, 49
Everett M., Howell S., 2001, PASP, 113, 1428
Fuhrmeister B., Schmitt J., 2003, A&A, 403, 247
Hebb L. et al., 2006, AJ, 131, 555
Irwin J. et al., 2009, ApJ, 701, 1436
Landolt A., 1992, AJ, 104, 340
Leggett S., 2000, ApJS, 82, 351
Lenz P., Breger M., 2005, CoAst, 146, 53
Leung K., Schneider D., 1978, AJ, 83, 618
Lopez-Morales M., Ribas I., 2005, ApJ, 131, 555
Lopez-Morales M. et al., 2006, ArXiv:astro-ph/0610225v1
Maceroni C., Montalbán J., 2004, A&A, 426, 577
Maceroni C., Rucinski S.M., 1997, PASP, 109, 782
Maceroni C. et al., 1994, A&A, 288, 529
Metcalf T. et al., 1996, ApJ, 456, 356
Mullan D., MacDonald J., 2001, ApJ, 559, 353
Norton A.J., et al., 2007, A&A, 467, 785
Pollacco D., et al. 2006, PASP, 118, 1407
Popper D., Ulrich R., 1977, ApJ, 212, L131
Pribulla T., Rucinski S., 2006, AJ 131, 2986
Pribulla T., Vanko M., Hambalek L., 2009, IBVS, No.5886
Prša A., Zwitter T., 2005, ApJ, 628, 426
Ribas I., 2003, A&A, 398, 239
Rosner R. et al., 1981, ApJ, 249, L5
Rucinski S.M., 1992, AJ, 103, 960
Rucinski S.M., 1984, A&A, 132, L9
Rucinski S.M., 2007, MNRAS, 382, 393
Rucinski S.M., Pribulla T., 2008, MNRAS, 388, 1831
Schlegel D., Finkbeiner D., Davis M., 1998, ApJ, 500, 525
Schmitt J., Fleming T., Giampapa M., 1995, ApJ, 450, 392
Stauffer J.R., Hartmann L.W., 1986, ApJS, 61, 531
Stepien K., 2006, Acta Astr., 56, 347
Stetson P., 2000, PASP, 112, 925
Torres G., Ribas I., 2002, ApJ, 567, 1140
VandenBerg D., Clem J., 2003, AJ, 126, 778
van Hamme W., 1993, AJ, 106, 2096
Vida K., Olah K., Kovari Zs., Bartus J., 2009, AIPS, 1094, 812
Vilhu O., Walter F., 1987, ApJ 321, 958
Voges W., Aschenbach B., Boller T., et al., 1999, A&A 349, 389
Weldrake D.T.F., Sackett P.D., Bridges T.J., Freeman K.C., 2004, AJ, 128, 736
Worden S.P., Schneeberg T.J., Giampapa M.S., 1981, ApJS, 46, 159
Wozniak P.R., Vestrand C.W., Akerlof R., et al., 2004, AJ, 127, 2436
Young T. et al., 2006, MNRAS, 370, 1529
Zacharias N., Monet D., Levine S., et al., 2005, AAS, 205, 4815